

Article - Human and Animal Health

Improved Antiproliferative Activity of Doxorubicin-Loaded Calcium Phosphate Nanoparticles Against Melanoma Cells

Igor Barbosa Lima^{1*}

<https://orcid.org/0000-0003-1171-5741>

Betania Mara Alvarenga¹

<https://orcid.org/0000-0002-6057-8280>

Priscila Izabel Santos de Tótar¹

<https://orcid.org/0000-0002-0102-5811>

Fernanda Boratto³

<https://orcid.org/0009-0008-6135-3383>

Elaine Amaral Leite³

<https://orcid.org/0000-0001-8812-3811>

Pedro Pires Goulart Guimaraes²

<https://orcid.org/0000-0003-4534-2779>

¹Universidade Federal de Minas Gerais, Instituto de Ciências Biológicas, Departamento de Morfologia, Belo Horizonte, Minas Gerais, Brasil; ²Universidade Federal de Minas Gerais, Instituto de Ciências Biológicas, Departamento de Fisiologia e Biofísica, Belo Horizonte, Minas Gerais, Brasil; ³Universidade Federal de Minas Gerais, Faculdade de Farmácia, Departamento de Produtos Farmacêuticos, Belo Horizonte, Minas Gerais, Brasil.

Editor-in-Chief: Paulo Vitor Farago

Associate Editor: Najeh Maissar Khalil

Received: 10-Aug-2022; Accepted: 18-Jul-2023

*Correspondence: limaigor6@gmail.com - (I.B.L.)

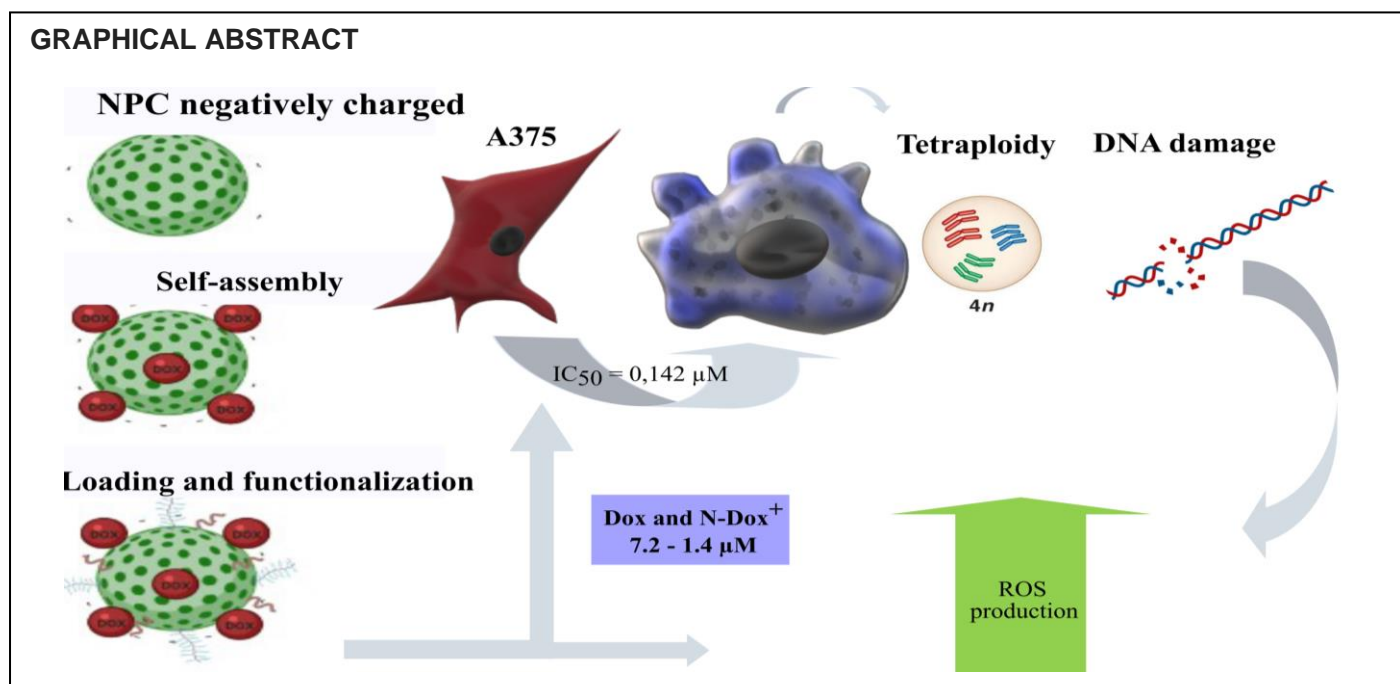
HIGHLIGHTS

- N-Dox has higher activity against A-375 cells than free doxorubicin.
- The formulation has higher selectivity indices than free doxorubicin.
- Treatment induced senescence and no colonies recovered after short-term exposure.

Abstract: The high incidence of melanoma has received significant attention. Despite advances in early detection and standard treatment options, new strategies that improve therapy with reduced side effects are highly desirable. Several studies have demonstrated the efficiency of doxorubicin (Dox) to treat melanoma, however, side effects limit its clinical use. Drug delivery systems, especially nanostructured ones, are a useful approach to enhance antitumor activity and reduce toxicity of drugs. Here, the use of calcium phosphate nanoparticles functionalized with Dox and hyaluronic acid (N-Dox) to enhance Dox antiproliferative activity is reported. The effects were accessed in A-375 melanoma cells, in which N-Dox IC₅₀ significantly decreased over 48 hours ($0.14 \pm 0.07 \mu\text{M}$) compared to free drug ($0.44 \pm 0.25 \mu\text{M}$) and showed selective action against A-375 when compared with HEK-293 cells. Treatment triggered DNA damage, increased nuclear area, and elicited senescent phenotype. Furthermore, it did not form colonies after 14 days of

incubation preceded by short exposure treatment. These preliminary results indicate that N-Dox hold promise for melanoma treatment, reducing the minimum effective dose and perhaps a reduction in the cost of treatment.

Keywords: Senescence; drug delivery; cytotoxicity; A-375.



INTRODUCTION

Cancer remains a major public health issue, being the second leading cause of death in the U.S., exceeded only by cardiac failure [1]. Melanoma is a class of skin cancer that develops quickly, invasively, has poor diagnosis [2,3] and, its occurrence is increasing over the years. The American Cancer Society informs that at least 99.780 new cases of melanoma were expected to be reported in 2022 [4].

Most melanoma cases are associated with a mutation that results in overexpression of B-raf proto-oncogene, concomitant with a reduction of p53 activity [5]. BRAFq enzyme acts as a modulator for cell cycle progression under external stimulus (e.g., growth factors and hormones). However, once the BRAFq gene expression is upregulated, this cell division pathway is triggered without external stimuli, what leads to uncontrolled cell proliferation. Due to this, BRAFq pathway has become a target for melanoma treatment, focusing on the development of drugs that act directly by blocking its activity [6].

On the other hand, some melanoma cases do not present BRAFq upregulation, what brings a research approach on alternative therapeutic targets [7]. Doxorubicin hydrochloride (Dox) is not currently used as a treatment protocol for melanoma [8], however several studies demonstrated Dox efficacy to treat it [9-11]. Despite the advances, clinical using of Dox is still a challenge because of a range of serious side effects occurring during treatment (nausea, headache, etc.) and long-term sequelae [12] that includes marked dose-dependent cardiotoxicity and nephrotoxicity [13,14].

In this context, the reduction of the effective dose becomes a therapeutic target of interest that can be achieved by nanotechnology [15,16]. Calcium phosphate nanoparticles (NPC), are composed by magnesium, calcium, and phosphorus, it has amorphous nature, spherical shape, average diameter of 149 nm, and are efficient in delivering drugs to different types of cells, such as macrophages and breast cancer cells [17,18].

NPC can be functionalized by hyaluronic acid (HA) as a strategy to increase targeting to cancer cells [19]. HA binds with CD44 receptor [20], which is overexpressed in several cancers, including melanoma [21,22]. Several studies demonstrate the effectiveness of the functionalization of solid nanoparticles with hyaluronic acid as a strategy to increase cell uptake due to the fact that this molecule interacts with CD44 receptors, thus, this interaction occurs more intensely in tumor cells overexpressing CD44 receptors [23-25]. Besides that, NPC can adsorb Dox (approximately 17.72%), which decreases zeta potential [18]. These characteristics are interesting to promote increased tumor retention by enhanced permeability and retention effect [26]. These findings are consistent with the antiproliferative activity of Dox loaded NPC observed against human breast cancer cells [18]. However, the possibility of being used as a therapeutic platform for

the treatment of melanoma has not yet been investigated. Based on that, the hypothesis that using Dox loaded NPC for drug delivery potentiates doxorubicin activity against melanoma cells was postulated.

The adsorption of Dox on NPC was performed followed by functionalization with hyaluronic acid, resulting in a formulation mentioned as N-Dox. N-Dox cytotoxic activity against melanoma cells (A-375 cell line - *Homo sapiens*) were accessed, as well as the investigation of the cytotoxicity mechanism.

MATERIAL AND METHODS

Synthesis of NPC and N-Dox preparation

NPC was synthesized using phosphate salts solutions at controlled pH in a semipermeable membrane system, 25 mm wide (Fisher Scientific, USA) as described by Alvarenga [17]. A suspension containing 0.4 mg of NPC was eluted to 380 μL of Milli-Q water, mixed to 20 μL of a 1.8 mM Dox (Sigma Aldrich, USA), and homogenized on vortex for 5 minutes to lead to Dox adsorption on NPC surface by self-assembly, purified through three consecutive cycles of washing and centrifugation [27], and functionalized by 200 μL of a 3% (v/v) solution of hyaluronic acid (HA) (Merck, Germany) at room temperature and resuspended in PBS. NPC samples were functionalized only with HA [18].

Dox loading and adsorption efficiency

The amount of Dox loaded on N-Dox was determined by high-performance liquid chromatography (HPLC) with a fluorescence detector as described by Boratto [28]. Three independent preparations were analyzed. To measure the concentration of Dox adsorbed, the pellet was resuspended in 200 μL of HCl at 0.5 mM, since acidification digests the material. The analyses were performed in a Waters chromatographer (Waters Instruments, USA). The percentage of the load was calculated based on the equation Equation (1):

$$\% \text{ of load} = \frac{(c \cdot 100)}{90} \quad (1)$$

where c is the concentration of Dox in the sample in μM and 90 is the initial concentration in μM .

In vitro drug release studies

To determine the release rate of doxorubicin from N-Dox, the dialysis bag technique was used as described by Krai [29]. 400 μL of N-Dox suspension was prepared in triplicate and after 0.5, 1, 3, 4, 6, 8, and 20 hours, samples of 200 μL were removed and the same volume of PBS was replaced to avoid an increase in the concentration of the medium. The aliquots were analyzed by HPLC as previously described.

Cell culture

All cell lines were cultivated in DMEM medium (Sigma Aldrich, USA), containing 10% fetal bovine serum (GIBCO BRL, USA) and 1% antibiotic solution 100 IU. mL^{-1} of penicillin and 100 $\mu\text{g} \cdot \text{mL}^{-1}$ of streptomycin (GIBCO BRL, USA) and kept in a humidified atmosphere with 5% CO_2 at 37 °C. A-375 and HEK-293 cell lines were kindly donated by Dr. Helen Lima del Puerto/UFMG – Brazil. Cells were authenticated and tested for infection by *Mycoplasma sp.* through PCR.

Cytotoxicity assessment

Cell proliferation was assessed by the colorimetric assay of sulforhodamine B 2-(3-diethylamino-6-diethylazaniumylidene-xanthen-9-yl)-5-sulfo-benzenesulfonate (SRB) (Sigma Aldrich, USA) [30]. A-375 cells were seeded at a density of 5×10^3 cells per well in 96-well plates and treated with NPC, N-Dox, and free Dox suspended in PBS by using eight serial dilutions (1: 5) with concentrations between 120 - 0.0 $\mu\text{g} \cdot \text{mL}^{-1}$, 1.42 - 0.0 μM , and 180 - 0.0 μM , respectively, and challenged for a period of 48 hours. The control group was treated only with PBS. NPC concentrations are expressed in $\mu\text{g} \cdot \text{mL}^{-1}$ due to the intrinsic difficulties of calculating nanoparticle molarity, being 0.6 $\mu\text{g} \cdot \text{mL}^{-1}$ the mass of NPC present in 0.14 μm of N-Dox. The spectrophotometric reading of the OD was performed at 510 nm in a multi-well plate reader Varioskan Lux (Thermo Fisher Scientific, USA).

Results were expressed as a percentage of cell viability as a function of concentration. The OD was normalized as the percentage of cell viability (% CV) considering the absorbance of the PBS-treated control (ODPBS) as 100% viability, according to the equation Equation (2):

$$\%CV = \frac{(100 \times OD)}{OD_{PBS}} \quad (2)$$

Values of inhibitory concentration for 50% of the cell population (IC₅₀) were calculated by non-linear regression using GraphPad Prism® software version 5.0 (GraphPad Software Inc, USA). The selectivity indices (SI) were calculated for each formulation as the ratio between the IC₅₀ of the HEK-293 cell line and the IC₅₀ of the A-375 cell line [31].

DNA quantification and evaluation of cell cycle

The quantification of DNA and analysis of the cell cycle were performed as described by Riccardi and Nicoletti [32]. Subsequently, cells were treated with concentrations referring to the 48 hours IC₅₀ (Dox = 0.44 µM, N-Dox = 0.14 µM and NPC = 0.6 µg.mL⁻¹). After 48 hours of treatment, cells were stained with hypotonic fluorochromic solution (HFS) and parameters were acquired by flow cytometer FACSCan® (BD Biosciences, USA) and analyzed in the software FlowJoX.0.7® (Tree Star Inc., USA).

Clonogenic assay

The long-term survival of A-375 cells after treatment with the formulations was accessed through the clonogenic assay [33]. Briefly, A-375 cells were seeded in 6-well plates at a density of 200 cells per well and incubated for 24 hours. After incubation, the cells received the treatments with the 48 hours IC₅₀ concentrations (Dox = 0.44 µM, N-Dox = 0.14 µM and NPC = 0.6 µg.mL⁻¹) for 4 hours and then the culture medium was renewed, incubated for 14 days and then fixed with 4% p-formaldehyde, washed, and stained with 0.1% violet crystal. The experiments were carried out in triplicate. Only colonies with at least 50 cells were considered and counted manually. The results are expressed as a fraction of survival, obtained by the equations below. Plating efficiency (PE) was determined as the ratio between the number of colonies formed in the well without the treatment and the number of cells seeded, multiplied by 100 Eq. (3). The surviving fraction (SF) was calculated by dividing the number of colonies formed after treatment by the number of seeded cells multiplied by PE Eq. (4).

$$PE = \frac{\text{Number of colonies formed by the untreated group}}{\text{Number of seeded cells}} \times 100 \quad (3)$$

$$SF = \frac{\text{Number of colonies formed by the untreated group}}{\text{Number of seeded cells} \times PE} \quad (4)$$

Nuclear morphometric analysis (NMA)

A-375 cells were seeded at a density of 5x10⁴ cells per well in 8 well Tek Chamber Slides (Thermo Fisher, USA) and incubated for 24 hours for stabilization. Cells were treated as described in topic *Cytotoxicity assessment*. and stained with Hoechst reagent (NucBlue™, USA) according to the manufacturer's instructions. The evaluation of nuclear morphometry was carried out by measurement of nuclear shape and area. These variables were used to calculate the nuclear irregularity index (NII), which is used to indicate the mechanism of cell death induced by treatments. The images were obtained in a confocal microscope LSM 880 (Zeiss, Germany) (magnification x 400) and analyzed using ImageJ software as described by Filippi-Chiella [34].

Statistical analysis

All experiments were carried out at least in triplicate. Data were expressed as mean \pm S.D. (standard deviation). Statistical analyzes were performed using GraphPad Prism software, version 5.0, GraphPad Software, Inc, USA. The normality of the data was ascertained by the Kruskal-Wallis test and the difference between means of treatments was accessed by One-way ANOVA with Tukey's multiple comparison test. Significant differences were considered at the level of $p \leq 0.05$.

RESULTS AND DISCUSSION

Characterization of nanoparticles

NPC used in this work were loaded with Dox through electrostatic interactions, in an aqueous medium to promote self-assembly and previously characterized [18]. It is a process less laborious, less costly and avoids the use of organic solvents (such as dimethyl sulfoxide) that can increase the toxicity of formulations [35]. The coating of the nanoparticles with HA also was carried out by adsorption, and this technique has been described as satisfactory for this purpose [36].

Dox quantification by HPLC was performed to confirm the loading observed previously. N-Dox showed a mean Dox concentration of $14.2 \pm 4.8 \mu\text{M}$ (this value was considered as the average concentration of Dox present in N-Dox for the subsequent experiments and calculations), regarding a mean load of $15.78 \pm 5.33\%$ (Figure 1.a), consistent with the values found previously [18]. Positively charged cerium oxide nanoparticles, with zeta potential ranging from -31.16 to 40.2 mV, can load to bovine serum albumin (negatively charged protein), since the zeta potential is positive [37]. The loading of Dox on the NPC in our study follows a similar pattern: negatively charged NPC (negative zeta potential) preforms electrostatic interactions with Dox, a cationic compound [38].

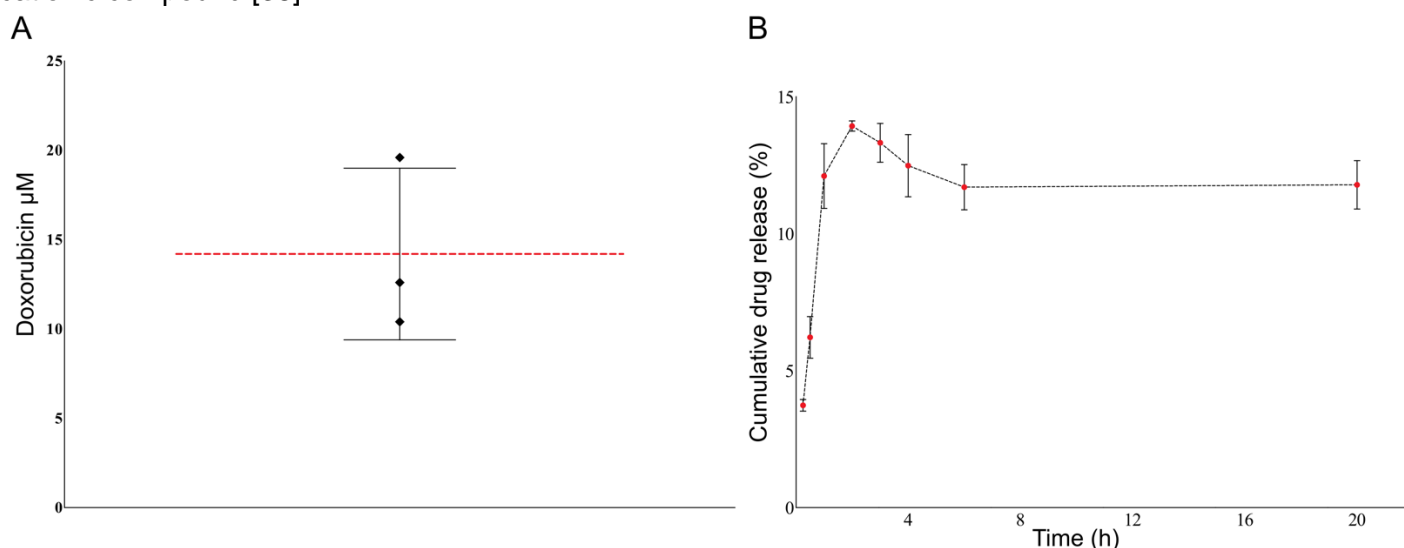


Figure 1. Concentration of Dox adsorbed on NPC. Analysis performed on HPLC after acid digestion (A); release/diffusion profile from N-Dox. Initial concentration 25.2 mg.mL^{-1} (B). Red dashed lines represent the average of the measurements, $n = 3$, \pm S.D.

The diffusion/release profile of Dox from N-Dox (Figure 1. b) shows a burst of release between 1 and 2 hours of incubation at pH 7.4, with a peak in approximately 2 hours ($13.9\% \pm 0.18$). This finding suggests that N-Dox is a drug delivery system with a slow-release rate, which likely provides constant drug release in the first hours, increasing the drug retention time. Nano formulations are expected to increase the drug retention time of Dox [39] and can influence the enhanced permeability and retention effect [40].

Cytotoxic activity

Dox can act in both, the cytoplasm and nucleus [41]. After its internalization, Dox is reduced to an unstable semiquinone that is transformed again into Dox, generating reactive oxygen species (ROS) [42]. On the other hand, Dox reach the nucleus, causes damage to topoisomerase II, and alters the expression of genes involved in DNA repair and cell cycle regulation [43].

A-375 cells presented remarkable morphological changes after treatments (Figure 2.a), consistent with dose-response cytotoxicity curves (Figure 2.b).

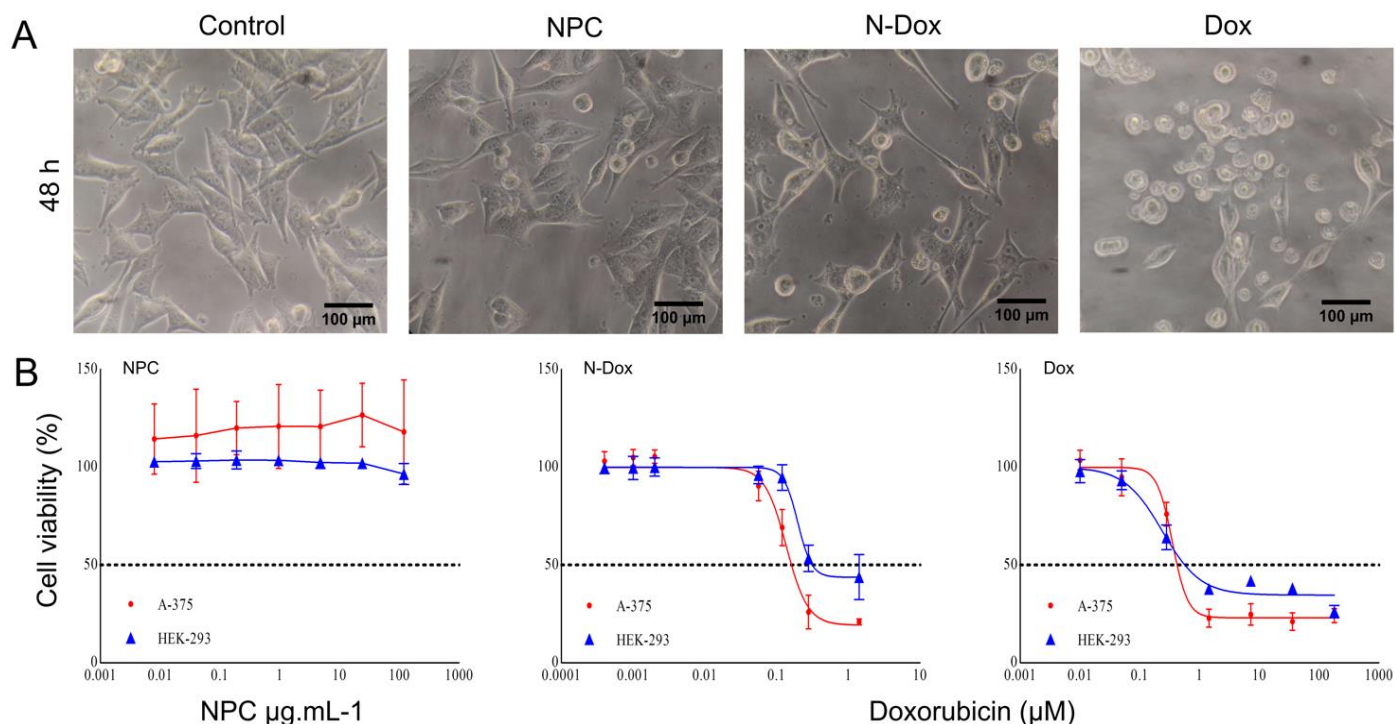


Figure 2. Antiproliferative activity of Control (PBS), NPC (0.6 µg.mL⁻¹), N-dox (0.14 µM), and Dox (0.44 µM) after 48 hours. Representative photomicrographs of the morphology of A-375 cells after treatment obtained under a phase contrast microscope, scale bars: 100 µm (A); Dose-response curves of cell lines A-375 and HEK-293 after treatment with Dox, N-Dox, and NPC for 48 hours (B).

Treatment with N-Dox for 48 hours significantly reduced the dose required (0.14 ± 0.07 µM) compared to free drug (0.44 ± 0.25 µM). The values are summarized in table 1. After 48 hours the cytotoxic effects of N-Dox increase, once this stage, there is a damage accumulation caused by Dox molecules slowly released from the nanoparticles, causing DNA damage (Figure 3.a). It was not possible to calculate the IC₅₀ of unloaded NPC since there was no significant reduction in cell viability after treatment.

Table 1. Values of IC₅₀ of Dox and N-Dox in cell lines A-375 and HEK-293 after 48 hours of treatment and selectivity indexes. Values were expressed as the average of 3 independent experiments ± S.D. and uncalculated values represented by "NC".

	A-375	HEK-293	
	IC ₅₀	IC ₅₀	SI
Dox	0.44 ± 0.25 µM	0.24 ± 0.12 µM	<1
N-Dox	$0.13 \pm 0,07$ µM	0.43 ± 0.22 µM	3.2
NPC	NC	NC	NC

In vitro models are efficient to access the security of new technologies and drive research promoting the policy of the three R's (replacement, reduction, and refinement) for using animals in research [44]. HEK-293 cells are a classic model for predicting drug safety and nephrotoxicity [45]. The selectivity indices (SI) (Dox = 0.54; N-Dox = 3.2) shows that N-Dox have selective cytotoxicity to A-375 when compared to HEK-293 cell line. Since health cells are less affected by N-Dox, that could represent reduced side effects hereafter, when it is *in vivo* tested.

Cell cycle assessment

To determine the predominant cell death mechanism over melanoma cells, the viability must be evaluated in line with cell cycle progression. Treatment with NPC did not cause any change in the cell cycle. Treatment with N-Dox (0.14 µM) and Dox (0.44 µM) in A-375 cells induce significant changes in cell cycle progression after 48 hours of treatment (Figure 3. b). A significant increase in DNA damage was observed, which is a strong indication of the occurrence of programmed cell death [46] and a reduction in the number

of diploid cells (G0/G1). There was no alteration in the number of cells in the S phase. Since no significant difference in cell cycle progression was observed after treatment with N-Dox, compared to the drug free form, it is presumable that loading doxorubicin to NPC as a platform for delivery, does not alter the Dox mechanism of action.

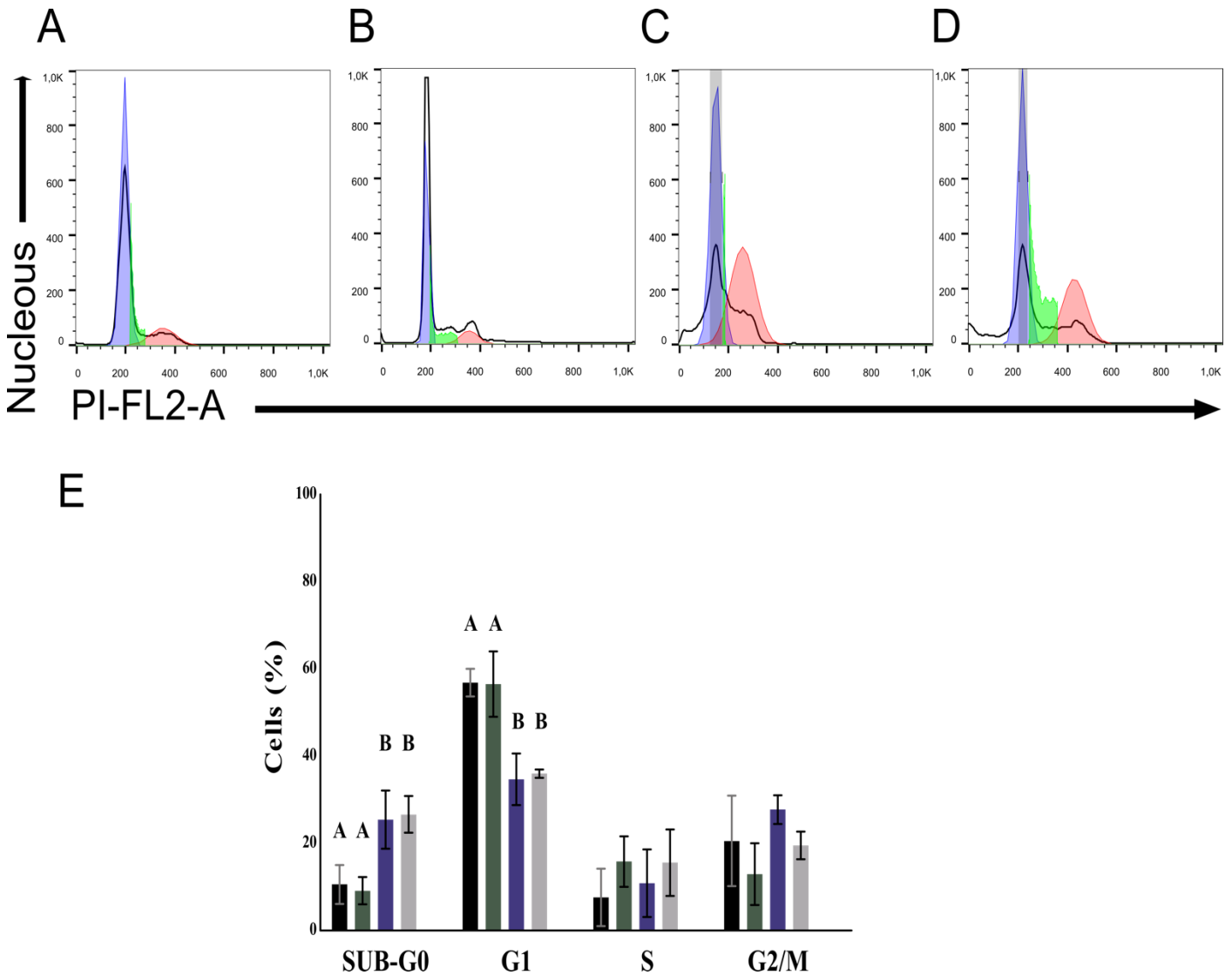


Figure 3. Effect of treatment with PBS (A), NPC (0.6 mg.ml⁻¹) (B), N-Dox (0.14 µM) (C), and Dox (0.44 µM) (D) to cell cycle of A-375 cells, counting of affected cells (E). Data expressed as mean ± S.D. obtained from three independent experiments carried out in duplicate, n = 6. Data compared by ANOVA and Dunnett's means test with a significance level at p < 0.05. The letters A and B show a significant difference between treatments.

Cell death pathway

The occurrence of tumor recurrence and multiple drug resistance is characterized by resistance to several drugs with different treatment targets [33]. The clonogenic assay simulates the effect of long-term treatment and tests the ability of a tumor cell to perform infinite cell divisions, even after exposure to a cytotoxic stimulus [33]. Our results showed that N-Dox administration was able to prevent the formation of A-375 cell colonies after 14 days of incubation, which indicates that the cells were not able to reverse the damage caused by short exposure period treatment [33]. NPC treatment formed colonies as well as control. Plating efficiency (PE) and surviving fractions are summarized in table 2.

Table 2. Clonogenic assay results showing the number of colonies (NC), plating efficiency (PE), and a surviving fraction (SF) of A-375 cells after treatment. Data expressed as mean \pm S.D. n = 3.

Treatment	NC	PE	SF
Dox	0 \pm 0,0	-	0 \pm 0,0
N-Dox	0 \pm 0,0	-	0 \pm 0,0
NPC	156 \pm 12,16	-	0,01 \pm 0,0
Control	178 \pm 5,03	89,2 \pm 2,51	0,01 \pm 0,0

To ascertain which cell death mechanism is activated by N-Dox, cell nuclei were stained by Hoechst (Figure 4.a) for subsequent Nuclear Morphometric Analysis [34]. Both Dox and N-Dox triggered the occurrence of large and regular nuclei in A-375 cells (64.2% \pm 2.7 for Dox and 68.8% \pm 12.8 for N-Dox) i.e., senescent cells (Figure 4.b). Cancer cells can enter a state of senescence after being exposed to chemotherapeutic agents [19,47] e.g., doxorubicin, which is a potent inducer of senescence in cancer cells [48]. This phenomenon is a desirable form of treatment for cancer known as therapy-induced senescence (TIS) as it stops the progression of tumors less aggressively [49], being considered a good strategy to stop melanoma development [50]. The ability to form colonies was completely inhibited suggesting the absence of cells capable of evading the senescence mechanism [51], since escaper cells are more invasive and form colonies faster [52].

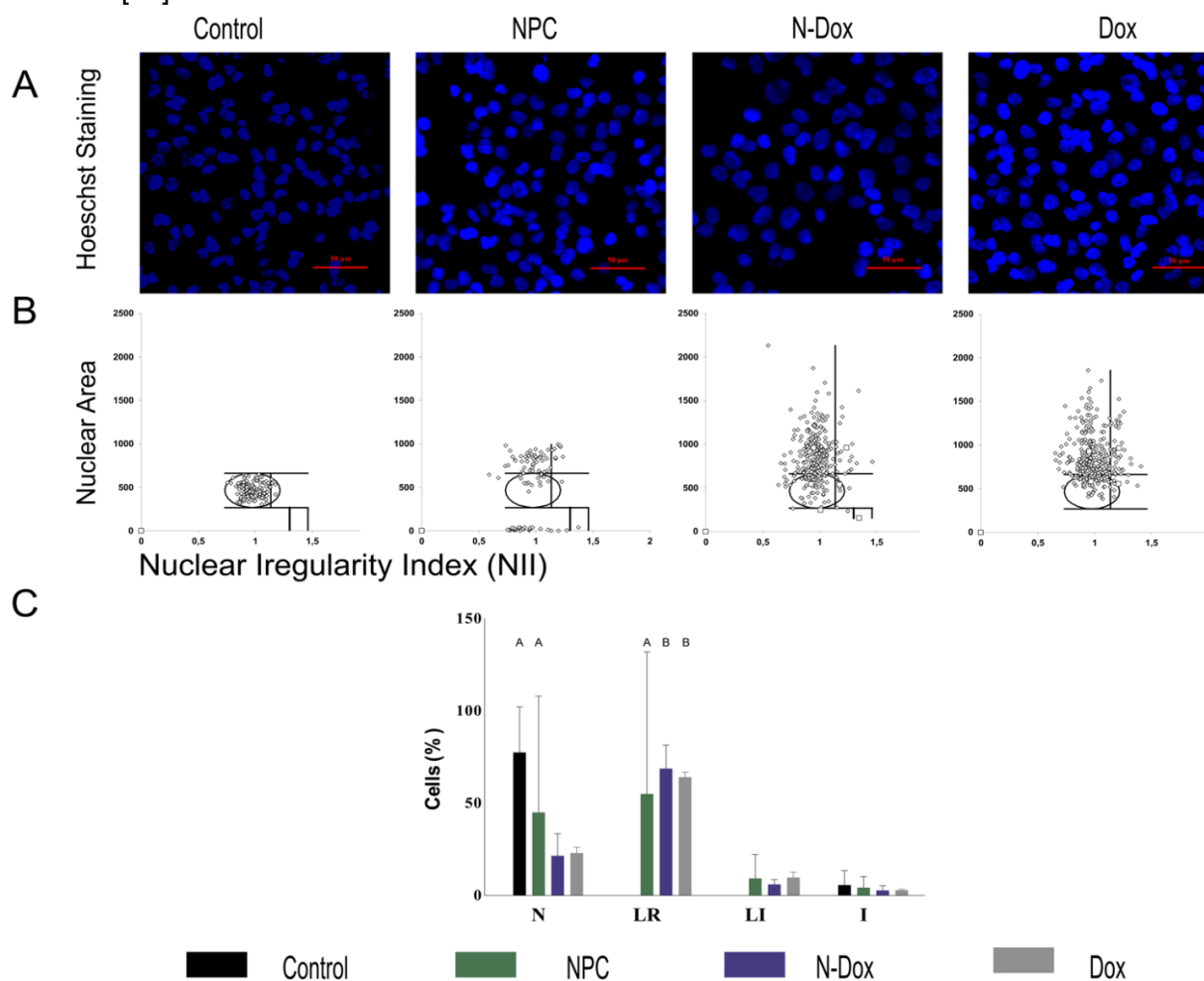


Figure 4. Nuclear Morphometric Analysis of A-375 cells treated as indicated. Nucleus was stained with Hoechst for confocal microscopy imaging; scale bars, 50 μ m; magnification, 400 x (A). Nuclear area (y-axis) and shape (x-axis) measured (B). Nuclei classified as N = normal; I = Irregular; LR = Large Regular, and LI = Large Irregular, showing the percentage of senescent nuclei (LR) (C). Results were compared by ANOVA and Tukey's mean comparison with a significance level at $p < 0.05$. Letters A and B indicate a significant difference between treatments, n = 6.

CONCLUSION

NPC has shown to be an efficient drug delivery system for Dox with a mean retention capacity of 15.78 % \pm 5.33 and, has a slow-release rate, which could provide a longer drug retention time in the circulation. N-Dox provided potentiation of Dox effect after 48 hours of treatment and elicited senescent phenotype. As no colonies were formed, after long-term survival assay, the absence of escaper cells is suggested. Our preliminary findings demonstrated that N-Dox has enhanced activity compared to Dox and selectivity. The quantification of the expression of the genes involved with the progression of the cell cycle is fundamental to confirm the absence of escapers cells. This approach will allow that the formulation has its effectiveness and safety assured. N-dox is promising as a potential treatment for melanoma that could reduce damage to patients and reduce treatment costs due to the smaller amount of drug used.

Funding This research was funded by PROEX-CAPES.

Acknowledgments I would like to thank everyone who directly or indirectly contributed to this research.

Conflicts of Interest: The authors declare no conflict of interest.

REFERENCES

1. Siegel RL, Miller KD, Jemal A. Cancer statistics, 2020. *CA Cancer J Clin.* 2020;70(1):7-30. Available from: <https://doi.org/10.3322/caac.21590>.
2. Fattore L, Costantini S, Malpicci D, Ruggiero CF, Ascierto PA, Croce CM, et al. MicroRNAs in melanoma development and resistance to target therapy. *Oncotarget.* 2017;8(13):22262-78. Available from: <https://doi.org/10.18632/oncotarget.14763>.
3. Lunkes VL, Palma TV, Assmann CE, Mostardeiro VB, Schetinger MRC, Morsch VMM, et al. Curcumin and Vinblastine Disturb Ectonucleotides Enzymes Activity and Promote ROS Production in Human Cutaneous Melanoma Cells. *Braz Arch Biol Technol.* 2022 09 Apr 65:1-9. Available from: <https://doi.org/10.1590/1678-4324-2022220187>.
4. Miller KD, Nogueira L, Devasia T, Mariotto AB, Yabroff R, Jemal A, et al. Cancer treatment and survivorship statistics, 2022. *CA Cancer J Clin.* 2022;72(5):409-36. Available from: <https://doi.org/10.3322/caac.21731>.
5. Larkin J, Chiarion-Sileni V, Gonzalez R, Grob JJ, Cowey CL, Lao CD, et al. Combined Nivolumab and Ipilimumab or Monotherapy in Untreated Melanoma. *N Engl J Med.* 2015;373(1):23-34. Available from: <https://doi.org/10.1056/NEJMoa1504030>.
6. Schadendorf D, Fisher DE, Garbe C, Gershenwald JE, Grob JJ, Halpern A, et al. Melanoma. *Nat Rev Dis Primer.* 2015;1(1):15003. Available from: <https://doi.org/10.1038/nrdp.2015.3>.
7. Hutchinson KE, Lipson D, Stephens PJ, Otto G, Lehmann BD, Lyle PL, et al. BRAF Fusions Define a Distinct Molecular Subset of Melanomas with Potential Sensitivity to MEK Inhibition. *Clin Cancer Res.* 2013;19(24):6696-702. Available from: <https://doi.org/10.1158/1078-0432.CCR-13-1746>.
8. Azevedo SJ, Melo AC, Roberts L, Caro I, Xue C, Wainstein A. First-line atezolizumab monotherapy in patients with advanced BRAF^{V600} wild-type melanoma. *Pigment Cell Melanoma Res.* 2021;34(5):973-7. Available from: <https://doi.org/10.1111/pcmr.12960>.
9. Molinaro R, Martinez JO, Zinger A, De Vita A, Storci G, Arrighetti N, et al. Leukocyte-mimicking nanovesicles for effective doxorubicin delivery to treat breast cancer and melanoma. *Biomater Sci.* 2020;8(1):333-41. Available from: <https://doi.org/10.1039/C9BM01766F>.
10. Romano S, Nappo G, Cali G, Wang SYS, Staibano S, D'Angelillo A, et al. Synergy between enzastaurin doxorubicin in inducing melanoma apoptosis. *Pigment Cell Melanoma Res.* 2013;26(6):900-11. Available from: <https://doi.org/10.1111/pcmr.12144>.
11. Yoncheva K, Merino M, Shenol A, Daskalov NT, Petkov PS, Vayssilov GN, et al. Optimization and in-vitro/in-vivo evaluation of doxorubicin-loaded chitosan-alginate nanoparticles using a melanoma mouse model. *Int J Pharm.* 2019;556:1-8. Available from: <https://doi.org/10.1016/j.ijpharm.2018.11.070>.
12. Rawat PS, Jaiswal A, Khurana A, Bhatti JS, Navik U. Doxorubicin-induced cardiotoxicity: An update on the molecular mechanism and novel therapeutic strategies for effective management. *Biomed Pharmacother.* 2021;139:111708. Available from: <https://doi.org/10.1016/j.biopha.2021.111708>.
13. Chatterjee K, Zhang J, Honbo N, Karliner JS. Doxorubicin Cardiomyopathy. *Cardiology.* 2010;115(2):155-62. Available from: <https://doi.org/10.1159/000265166>.
14. Teymouri M, Farzaneh H, Badiie A, Golmohammadzadeh S, Sadri K, Jaafari MR. Investigation of Hexadecylphosphocholine (miltefosine) usage in Pegylated liposomal doxorubicin as a synergistic ingredient: In vitro and in vivo evaluation in mice bearing C26 colon carcinoma and B16F0 melanoma. *Eur J Pharm Sci.* 2015;80:66-73. Available from: <https://doi.org/10.1016/j.ejps.2015.08.011>.
15. Klochkov SG, Neganova ME, Nikolenko VN, Chen K, Somasundaram SG, Kirkland CE, et al. Implications of nanotechnology for the treatment of cancer: Recent advances. *Semin Cancer Biol.* 2021;69:190-9. Available from: <https://doi.org/10.1016/j.semcancer.2019.08.028>.

16. Filho IK, Machado CS, Diedrich CK, Karam TK, Nakamura CV, Khalil NM, et al. Optimized chitosan-coated gliadin nanoparticles improved the hesperidin cytotoxicity over tumor cells. *Braz Arch Biol Technol*. 2021 May 20 64: 1-14. Available from: <https://doi.org/10.1590/1678-4324-75years-2021200795>.
17. Alvarenga BM, Melo MN, Frézard F, Demicheli C, Gomes JMM, da Silva JBB, et al. Nanoparticle phosphate-based composites as vehicles for antimony delivery to macrophages: possible use in leishmaniasis. *J Mater Chem B*. 2015;3(48):9250-9. Available from: <https://doi.org/10.1039/C5TB00376H>.
18. Priscila Izabel Santos de Totaro. Multifunctional phosphate based nanoparticles as a platform for imaging, targeting and doxorubicin delivery to human breast cancer CD44+ cells. Preprint. Published online 2021. Available from: <https://doi.org/10.1101/2021.11.08.467718>.
19. Assaraf YG, Brozovic A, Gonçalves AC, Jurkovicova D, Linē A, Machuqueiro M, et al. The multi-factorial nature of clinical multidrug resistance in cancer. *Drug Resist Updat*. 2019;46:100645. Available from: <https://doi.org/10.1016/j.drup.2019.100645>.
20. Aruffo A, Stamenkovic I, Melnick M, Underhill CB, Seed B. CD44 is the principal cell surface receptor for hyaluronate. *Cell*. 1990;61(7):1303-13. Available from: [https://doi.org/10.1016/0092-8674\(90\)90694-A](https://doi.org/10.1016/0092-8674(90)90694-A).
21. Dietrich A, Tanczos E, Vanscheidt W, Schöpf E, Simon JC. High CD44 surface expression on primary tumours of malignant melanoma correlates with increased metastatic risk and reduced survival. *Eur J Cancer*. 1997;33(6):926-30. Available from: [https://doi.org/10.1016/S0959-8049\(96\)00512-6](https://doi.org/10.1016/S0959-8049(96)00512-6).
22. Hou X, Tao Y, Li X, Pang Y, Yang C, Jiang G, et al. CD44-Targeting Oxygen Self-Sufficient Nanoparticles for Enhanced Photodynamic Therapy Against Malignant Melanoma. *Int J Nanomedicine*. 2020;Volume 15:10401-16. Available from: <https://doi.org/10.2147/IJN.S283515>.
23. An T, Zhang C, Han X, Wan G, Wang D, Yang Z, et al. Hyaluronic acid-coated poly (β -amino) ester nanoparticles as carrier of doxorubicin for overcoming drug resistance in breast cancer cells. *RSC advances*, 6(45): 38624-36. Available from: <https://doi.org/10.1039/C6RA03997A>.
24. Gupta B, Poudel BK, Ruttala HB, Regmi S, Pathak S, Gautam M, et al. Hyaluronic acid-capped compact silica-supported mesoporous titania nanoparticles for ligand-directed delivery of doxorubicin. *Acta biomater*, 80: 364-77. Available from: <https://doi.org/10.1016/j.actbio.2018.09.006>.
25. Wang S, Zhang J, Wang Y, Chen M. Hyaluronic acid-coated PEI-PLGA nanoparticles mediated co-delivery of doxorubicin and miR-542-3p for triple negative breast cancer therapy. *Nanomed.: Nanotechnol. Biol. Med.* 12(2): 411-20. Available from: <https://doi.org/10.1016/j.nano.2015.09.014>.
26. Liu X, Chen Y, Li H, Huang N, Jin Q, Ren K, et al. Enhanced Retention and Cellular Uptake of Nanoparticles in Tumors by Controlling Their Aggregation Behavior. *ACS Nano*. 2013;7(7):6244-57. Available from: <https://doi.org/10.1021/nn402201w>.
27. Langer K, Balthasar S, Vogel V, Dinauer N, von Briesen H, Schubert D. Optimization of the preparation process for human serum albumin (HSA) nanoparticles. *Int J Pharm*. 2003;257(1-2):169-80. Available from: [https://doi.org/10.1016/S0378-5173\(03\)00134-0](https://doi.org/10.1016/S0378-5173(03)00134-0).
28. Boratto FA, Franco MS, Barros ALB, Cassali GD, Malachias A, Ferreira LAM, et al. Alpha-tocopheryl succinate improves encapsulation, pH-sensitivity, antitumor activity and reduces toxicity of doxorubicin-loaded liposomes. *Eur J Pharm Sci*. 2020;144:105205. Available from: <https://doi.org/10.1016/j.ejps.2019.105205>.
29. Krai J, Beckenkamp A, Gaelzer MM, Pohlmann AR, Guterres SS, Filippi-Chiela EC, et al. Doxazosin nanoencapsulation improves its in vitro antiproliferative and anticlonogenic effects on breast cancer cells. *Biomed Pharmacother*. 2017;94:10-20. Available from: <https://doi.org/10.1016/j.biopha.2017.07.048>.
30. Vichai V, Kirtikara K. Sulforhodamine B colorimetric assay for cytotoxicity screening. *Nat Protoc*. 2006;1(3):1112-6. doi:10.1038/nprot.2006.179.
31. Chuang CH, Cheng TC, Leu YL, Chuang KH, Tzou SC, Chen CS. Discovery of Akt Kinase Inhibitors through Structure-Based Virtual Screening and Their Evaluation as Potential Anticancer Agents. *Int J Mol Sci*. 2015;16(2):3202-12. Available from: <https://doi.org/10.3390/ijms16023202>.
32. Riccardi C, Nicoletti I. Analysis of apoptosis by propidium iodide staining and flow cytometry. *Nat Protoc*. 2006;1(3):1458-61. Available from: <https://doi.org/10.1038/nprot.2006.238>.
33. Franken NAP, Rodermond HM, Stap J, Haveman J, van Bree C. Clonogenic assay of cells in vitro. *Nat Protoc*. 2006;1(5):2315-9. Available from: <https://doi.org/10.1038/nprot.2006.339>.
34. Filippi-Chiela EC, Oliveira MM, Jurkovski B, Callegari-Jacques SM, Silva VD da, Lenz G. Nuclear Morphometric Analysis (NMA): Screening of Senescence, Apoptosis and Nuclear Irregularities. Lebedeva IV, ed. *PLoS ONE*. 2012;7(8):e42522. Available from: <https://doi.org/10.1371/journal.pone.0042522>.
35. Syed M, Skonberg C, Hansen SH. Effect of some organic solvents on oxidative phosphorylation in rat liver mitochondria: Choice of organic solvents. *Toxicol In Vitro*. 2013;27(8):2135-41. doi:10.1016/j.tiv.2013.09.010
36. Barbault-Foucher S, Gref R, Russo P, Guechot J, Bochot A. Design of poly- ϵ -caprolactone nanospheres coated with bioadhesive hyaluronic acid for ocular delivery. *J Controlled Release*. 2002;83(3):365-75. Available from: [https://doi.org/10.1016/S0168-3659\(02\)00207-9](https://doi.org/10.1016/S0168-3659(02)00207-9).
37. Patil S, Sandberg A, Heckert E, Self W, Seal S. Protein adsorption and cellular uptake of cerium oxide nanoparticles as a function of zeta potential. *Biomaterials*. 2007;28(31):4600-7. Available from: <https://doi.org/10.1016/j.biomaterials.2007.07.029>.

38. Zhang L, Zhang P, Zhao Q, Zhang Y, Cao L, Luan Y. Doxorubicin-loaded polypeptide nanorods based on electrostatic interactions for cancer therapy. *J Colloid Interface Sci.* 2016;464:126-36. Available from: <https://doi.org/10.1016/j.jcis.2015.11.008>.
39. Zaharudin NS, Mohamed Isa ED, Ahmad H, Abdul Rahman MB, Jumbri K. Functionalized mesoporous silica nanoparticles templated by pyridinium ionic liquid for hydrophilic and hydrophobic drug release application. *J Saudi Chem Soc.* 2020;24(3):289-302. Available from: <https://doi.org/10.1016/j.jscs.2020.01.003>.
40. Iyer AK, Khaled G, Fang J, Maeda H. Exploiting the enhanced permeability and retention effect for tumor targeting. *Drug Discov Today.* 2006;11(17-18):812-8. Available from: <https://doi.org/10.1016/j.drudis.2006.07.005>.
41. Jackson TL. Intracellular Accumulation and Mechanism of Action of Doxorubicin in a Spatio-temporal Tumor Model. *J Theor Biol.* 2003;220(2):201-13. Available from: <https://doi.org/10.1006/jtbi.2003.3156>.
42. Keizer HG, Pinedo HM, Schuurhuis GJ, Joenje H. Doxorubicin (adriamycin): A critical review of free radical-dependent mechanisms of cytotoxicity. *Pharmacol Ther.* 1990;47(2):219-31. Available from: [https://doi.org/10.1016/0163-7258\(90\)90088-J](https://doi.org/10.1016/0163-7258(90)90088-J).
43. Thorn CF, Oshiro C, Marsh S, Hernandez-Boussard T, McLeod H, Klein TE, et al. Doxorubicin pathways: pharmacodynamics and adverse effects. *Pharmacogenet Genomics.* 2011;21(7):440-6. Available from: <https://doi.org/10.1097/FPC.0b013e32833ffb56>.
44. Goh JY, Weaver RJ, Dixon L, Platt NJ, Roberts RA. Development and use of in vitro alternatives to animal testing by the pharmaceutical industry 1980–2013. *Toxicol Res.* 2015;4(5):1297-307. Available from: <https://doi.org/10.1039/C5TX00123D>.
45. Cezar GG. Can human embryonic stem cells contribute to the discovery of safer and more effective drugs? *Curr Opin Chem Biol.* 2007;11(4):405-409. Available from: <https://doi.org/10.1016/j.cbpa.2007.05.033>.
46. Bortner CD, Oldenburg NBE, Cidlowski JA. The role of DNA fragmentation in apoptosis. *Trends Cell Biol.* 1995;5(1):21-26. Available from: [https://doi.org/10.1016/S0962-8924\(00\)88932-1](https://doi.org/10.1016/S0962-8924(00)88932-1).
47. Sikora E, Czarnecka-Herok J, Bojko A, Sunderland P. Therapy-induced polyploidization and senescence: Coincidence or interconnection? *Semin Cancer Biol.* Published online December 2020:S1044579X20302534. Available from: <https://doi.org/10.1016/j.semcancer.2020.11.015>.
48. Bojko A, Czarnecka-Herok J, Charzynska A, Dabrowski M, Sikora E. Diversity of the Senescence Phenotype of Cancer Cells Treated with Chemotherapeutic Agents. *Cells.* 2019;8(12):1501. Available from: <https://doi.org/10.3390/cells8121501>.
49. Nardella C, Clohessy JG, Alimonti A, Pandolfi PP. Pro-senescence therapy for cancer treatment. *Nat Rev Cancer.* 2011;11(7):503-511. Available from: <https://doi.org/10.1038/nrc3057>.
50. Collado M, Gil J, Efeyan A, Guerra C, Schuhmacher AJ, Barradas M, et al. Senescence in premalignant tumours. *Nature.* 2005;436(7051):642-642. Available from: <https://doi.org/10.1038/436642a>.
51. Sabisz M, Skladanowski A. Cancer stem cells and escape from drug-induced premature senescence in human lung tumor cells: Implications for drug resistance and in vitro drug screening models. *Cell Cycle.* 2009;8(19):3208-3217. Available from: <https://doi.org/10.4161/cc.8.19.9758>.
52. Milanovic M, Fan DNY, Belenki D, Däbritz JHM, Zhao Z, Yu Y, et al. Senescence-associated reprogramming promotes cancer stemness. *Nature.* 2018;553(7686):96-100. Available from: <https://doi.org/10.1038/nature25167>.



© 2023 by the authors. Submitted for possible open access publication under the terms and conditions of the Creative Commons Attribution (CC BY NC) license (<https://creativecommons.org/licenses/by-nc/4.0/>).